01 Aug 2010

A Molecular Dynamics Study on the Transport of a Charged Biomolecule in a Polymeric Adsorbent Medium and Its Adsorption onto a Charged Ligand

Enrico Riccardi

Jee-Ching Wang
Missouri University of Science and Technology, jcwang@mst.edu

Athanasios I. Liapis
Missouri University of Science and Technology, ail@mst.edu

Recommended Citation

E. Riccardi et al., "A Molecular Dynamics Study on the Transport of a Charged Biomolecule in a Polymeric Adsorbent Medium and Its Adsorption onto a Charged Ligand," *Journal of Chemical Physics*, vol. 133, no. 8, American Institute of Physics (AIP), Aug 2010.
The definitive version is available at https://doi.org/10.1063/1.3473930

A molecular dynamics study on the transport of a charged biomolecule in a polymeric adsorbent medium and its adsorption onto a charged ligand

E. Riccardi, J.-C. Wang, and A. I. Liapis

Citation: The Journal of Chemical Physics **133**, 084904 (2010); doi: 10.1063/1.3473930
View online: https://doi.org/10.1063/1.3473930
View Table of Contents: http://aip.scitation.org/toc/jcp/133/8
Published by the American Institute of Physics

A molecular dynamics study on the transport of a charged biomolecule in a polymeric adsorbent medium and its adsorption onto a charged ligand

E. Riccardi,[a] J.-C. Wang, and A. I. Liapis[b]
Department of Chemical and Biological Engineering, Missouri University of Science and Technology, 400 West 11th Street, Rolla, Missouri 65409-1230, USA

(Received 3 June 2010; accepted 1 July 2010; published online 26 August 2010)

The transport of a charged adsorbate biomolecule in a porous polymeric adsorbent medium and its adsorption onto the covalently immobilized ligands have been modeled and investigated using molecular dynamics modeling and simulations as the third part of a novel fundamental methodology developed for studying ion-exchange chromatography based bioseparations. To overcome computational challenges, a novel simulation approach is devised where appropriate atomistic and coarse grain models are employed simultaneously and the transport of the adsorbate is characterized through a number of locations representative of the progress of the transport process. The adsorbate biomolecule for the system studied in this work changes shape, orientation, and lateral position in order to proceed toward the site where adsorption occurs and exhibits decreased mass transport coefficients as it approaches closer to the immobilized ligand. Furthermore, because the ligands are surrounded by counterions carrying the same type of charge as the adsorbate biomolecule, it takes the biomolecule repeated attempts to approach toward a ligand in order to displace the counterions in the proximity of the ligand and to finally become adsorbed. The formed adsorbate-ligand complex interacts with the counterions and polymeric molecules and is found to evolve slowly and continuously from one-site (monovalent) interaction to multisite (multivalent) interactions. Such a transition of the nature of adsorption reduces the overall adsorption capacity of the ligands in the adsorbent medium and results in a type of surface exclusion effect. Also, the adsorption of the biomolecule also presents certain volume exclusion effects by not only directly reducing the pore volume and the availability of the ligands in the adjacent regions, but also causing the polymeric molecules to change to more compact structures that could further shield certain ligands from being accessible to subsequent adsorbate molecules. These findings have significant practical implications to the design and construction of polymeric porous adsorbent media for effective bioseparations and to the synthesis and operation of processes employed in the separation of biomolecules. The modeling and analysis methods presented in this work could also be suitable for the study of biocatalysis where an enzyme is immobilized on the surface of the pores of a porous medium.
 [doi:10.1063/1.3473930]

I. INTRODUCTION

The important advances that have taken place in the fields of molecular biology and separation science in the past 25 years have contributed significantly in the development of large-scale production of diagnostics and biotherapeutics. In downstream purification and separation of bioactive molecules, the capture step serves the dual purpose of removing the bulk impurities and concentrating the product of interest. Because of this, ion-exchange chromatography has become a very important separation method in downstream purification for the isolation of peptides, enzymes, and proteins.[1–16] The affinity groups/ligands are either positively or negatively charged groups and are most often linked to the base matrix via a polymeric extender[3,6,7,14–16] because of the positive effect caused by the extender and which is extensively discussed in the literature.[3,6–16] The porous polymer layer grafted on the surface of the pores of the base matrix increases the effective interactive volume as well as the steric availability of the affinity groups/ligands for the biomolecule to be adsorbed; this in turn could increase the mass transfer rate as well as the total capacity available.

In the process used for the construction of porous polymer adsorbent media,[3,6–8,14–16] stage I concerns itself with the construction[14] of the porous polymer layers formed from the mutual interaction of the polymeric extender molecules which are grafted on the surface of the pores of the base matrix, while stage II involves[15,16] the immobilization of the affinity groups/ligands on the surface of the pores of the immobilized porous polymer layers. The adsorption process which involves (i) the transport mechanisms of the charged adsorbate biomolecules of interest in the porous polymeric

[a]Present address: Theoretische Physikalische Chemie, Technische Universität Darmstadt, Petersenstrasse 20, 64287 Darmstadt, Germany.
[b]Author to whom correspondence should be addressed. Electronic mail: ail@mst.edu. Tel.: (573) 341-4414. FAX: (314) 966-2181.

adsorbent medium and (ii) the interaction mechanisms involved in the adsorption of the adsorbate molecules onto the immobilized affinity groups/ligands are considered to represent stage III in the study of the separation of biomolecules by ion-exchange adsorption employing polymeric adsorbent particles whose formation involves stages I and II. Riccardi *et al.*[14] recently presented a methodology which enables one to (i) construct through molecular dynamics (MD) modeling and simulations different porous polymeric media and (ii) characterize the pore structure of the constructed porous polymeric media with respect to distributions of pore size, pore surface area, pore volume, and pore connectivity. Then if the size of the desired adsorbate molecule to be separated from a mixture of species is known and the size of the affinity group/ligand that will be immobilized on the surface of the pores of the polymeric structures in order to form the adsorbent medium that will be used to realize the separation of the adsorbate molecule by adsorption is also known, an approach[14] has been constructed and presented by which the porous polymeric medium having the structural characteristics that could potentially produce the most effective porous polymeric adsorbent medium could be selected from a set of different porous polymeric media. This work of Riccardi *et al.*[14] thus provides a methodology for modeling, designing, constructing, characterizing, and selecting the appropriate porous polymeric structure to be used for the immobilization of the desired affinity groups/ligands and represents a theoretical method for studying and predicting the behavior of stage I. After the selection of the most promising porous polymeric structure has taken place, then the surfaces of the pores of the polymeric medium are activated and after that the process of the immobilization of the selected affinity groups/ligands onto the activated pore surfaces commences. More recently, Riccardi *et al.*[15,16] also presented a theoretical approach[15,16] which enables one to (i) model and study the activation of the pore surfaces and the immobilization of the selected affinity groups/ligands onto the activated pore surfaces through the use of MD modeling and simulation methods, (ii) determine the spatial distributions of (a) the density of the immobilized affinity groups/ligands, (b) the counterions, (c) the local nonelectroneutrality, and (iii) analyze and characterize the structure of the porous adsorbent medium composed of the polymeric chains and the immobilized charged ligands. Furthermore, we have used this methodology[15,16] to investigate and study the immobilization of charged ligands onto the activated surfaces of the pores formed by the interaction of dextran polymer chains, the spatial distributions of the dextran monomers, charged ligands, and counterions under different ligand loadings, as well as the modifications in the porous dextran polymer structure due to the presence of the charged ligands. Thus, our recent works[15,16] represent a theoretical method for studying and predicting the behavior of stage II. These works[14–16] together have established a methodology able to construct and analyze the structure of different porous adsorbent media and also provided a procedure and criteria for selecting the structure of the porous adsorbent medium that could be particularly effective for the transport and adsorption of certain types of adsorbate biomolecules depending on the size of their hydrodynamic diameter. Both microscopic and macroscopic modeling studies[14–24] indicate that the transport and adsorption of adsorbate molecules are expected to be more efficient when the porous adsorbent medium has a high surface area, sufficiently large pores (the size of the pores is sufficient) to accommodate properly adsorbate molecules and also facilitate effectively the transport of the adsorbate molecules even after adsorption on the pore surfaces has occurred, and a high pore connectivity so that the adsorbate molecules can be effectively transported from the outer surface of the porous adsorbent medium to the interior porous regions of the medium, and, thus, utilize effectively the immobilized affinity groups/ligands. It is important to mention here that our recent microscopic modeling studies[15,16] have shown that the spatial distribution of the density of immobilized charged ligands in ion-exchange adsorbent particles is most likely nonuniform and the adsorbent particles also exhibit local nonelectroneutrality. The concept of nonuniformity in the spatial distribution of the density of immobilized charged ligands was used in a multiscale[24] modeling study where nonuniform functional forms describing the spatial distribution of immobilized ligands in porous spherical adsorbent particles were constructed based on results obtained from microscopic modeling and were then employed in a macroscopic[24] model that could describe the transport and adsorption of a single protein in different porous adsorbent media. The results obtained from the macroscopic model indicate that inner radial humps in the concentration profile of the single adsorbed protein in the particles could occur when the functional forms for the nonuniform spatial density distributions of the immobilized ligands have certain mathematical properties.[24] The results are very interesting and important because inner radial humps in the concentration profile of different adsorbed proteins have been measured experimentally[12,25] and can have implications with respect to the rates and system efficiencies at which adsorption separations could be performed.[4,5,9,12,24,25] Furthermore, the results of the multiscale[24] modeling study have indicated an experimental method by which the spatial density distribution of the immobilized ligands in porous adsorbent particles could be determined, and such measurements could also be used for quality control of the adsorbent medium.

In this work, the mass transport of the charged adsorbate biomolecule, desmopressin, and its adsorption onto the immobilized charged ligand, mercaptopropionic acid, on the surface of the pores of an adsorbent medium that has an intermediate[16] dextran surface density are studied by conducting MD simulations with potential models containing explicit atomistic features. This work is considered to provide a methodology for studying the behavior of stage III.

II. SYSTEM FORMULATION AND SIMULATION MODELS AND METHODS

In the present work which considers stage III, the transport and adsorption of a charged biomolecule onto the charged ligands immobilized on a representative porous

polymeric dextran layer selected from our previous works[14–16] concerning stages I and II are studied by conducting MD simulations. Desmopressin has been selected to be the charged adsorbate biomolecule which is a synthetic analogue of the neurohypophyseal peptide hormone vasopressin and has high antidiuretic and antibleeding potencies.[26] The desmopressin molecule has nine amino acid residues bonded together in the following sequence:

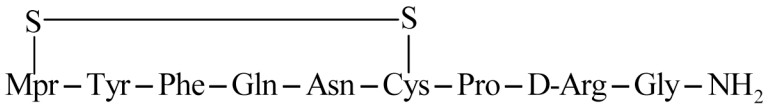

Its chemical structure and ball model representation are shown in Fig. 1(a). Considering the hydrodynamic diameter of desmopressin (~12 Å) and other factors discussed previously in Refs. 14–16, the porous adsorbent medium presented in Ref. 16 that has an intermediate dextran surface density provides a suitable porous structure for the transport and adsorption of desmopressin because it has high pore connectivity and large in diameter pores (up to 100 Å) which could possibly accommodate several desmopressin molecules and have continuous long pathway lengths along the direction of net transport (z axis). Mercaptopropionic acid ($HSCH_2CH_2COO^-$) (Ref. 7) is selected as the charged ligand in the present work for its similar dimension and mass and same net charge as the ligand considered in our previous works.[15,16] From the point of view that the ligand molecules immobilized on the dextran chains are the adsorption sites for the biomolecule, the dextran chains qualify to be considered as the pore surface and the porous structure of the dextran layer is thus formed and determined by mainly the mutual interactions between the dextran chains that, unlike solid porous materials, have substantial structural flexibility. As a result, the model simulation system, shown in Fig. 1 and like the actual system, is multicomponent, porous, and inhomogeneous with complex geometries and dynamics.

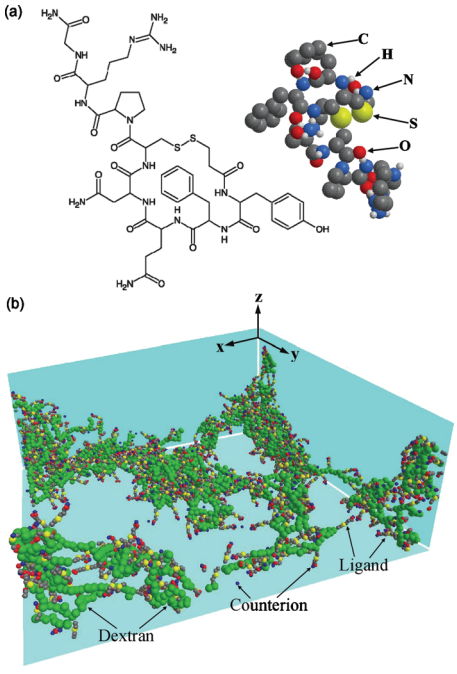

FIG. 1. A ball model of (a) the desmopressin molecule equilibrated in a bulk solution and its chemical structure and (b) the tilted top-down view of the porous polymeric dextran layer which is completely submerged in an aqueous solution and where agarose and water are not shown for visual clarity.

In order to obtain new insights at the molecular level concerning the mechanistic and dynamic aspects of biomolecular transport and adsorption in a nonrigid polymeric adsorbent medium, simulation potential models containing explicit atomistic features are needed. Here, only a brief explanation is given for those simulation models whose details have been available in our prior work[14–16] and in the references cited. The system is constructed with 20 dextran chains grafted on a nonflat surface that is represented by the following model:[14–16]

$$U_{is}(x,y,z) = 2\pi\varepsilon_{is}\left(\frac{\sigma_{is}}{R_{0s}}\right)^2\left[\frac{2}{5}\left(\frac{\sigma_{is}}{z_s}\right)^{10} - \left(\frac{\sigma_{is}}{z_s}\right)^4 - \frac{\sqrt{2}}{3\left(\frac{R_{0s}}{\sigma_{is}}\right)\left(\frac{z_s}{\sigma_{is}} + \frac{0.61}{\sqrt{2}}\frac{R_{0s}}{\sigma_{is}}\right)^3}\right], \tag{1a}$$

$$z_s = z - a\left[2 + \cos\left(\frac{2\pi}{b}x\right) + \cos\left(\frac{2\pi}{b}y\right)\right], \tag{1b}$$

where U_{is} is the interaction potential energy between the model surface and a particle i at (x,y,z) whose size and interaction strength are denoted by σ_i and ε_i. The interaction parameters are determined by the Lorentz–Berthelot mixing rule $\sigma_{is}=(1/2)(\sigma_i+R_{0s})$ and $\varepsilon_{is}=\sqrt{\varepsilon_i\varepsilon_{0s}}$, where R_{0s} and ε_{0s} represent the equilibrium distance and the interaction strength between agarose monomers. Along the lateral x and y axes of the simulation box, the linear dimensions are 202 $\times$ 202 Å^2 and periodic boundary conditions are applied. Grafted at one end onto the agarose surface, the dextran chains are 40 monomers long of which 5% have side branches that are one or two monomers in length.[14–16] For

computational efficiency and for structural consistency to enable comparison with previous results, a coarse grain M3B model developed and employed earlier[14–16,27] is retained in this work. This model represents each glucose monomer with three coarse grain beads denoted as B1, B4, and B6 and located in correspondence to the C1, C4, and C6 carbon atoms. It treats the bending and torsional motions among consecutive M3B beads with $U_b(\theta)=(1/2)k_\theta(\theta_i-\theta_0)^2$ and $U_{\text{tor}}(\phi)=\Sigma_{j=1}^{3}(1/2)B_j[1+\cos(j\phi-\phi_j^0)]$, respectively, for proper conformational representation, and the nonbonded interactions between M3B beads with the Morse potential[14–16]

$$U_{\text{nb}}(r_{ij})=D_{0,ij}\left\{\left[\exp\left(-0.5\alpha_{ij}\left(\frac{r_{ij}}{R_{0,ij}}-1\right)\right)-1\right]^2-1\right\}, \tag{2}$$

where r_{ij} is the distance between two dextran beads, $R_{0,ij}$ is the distance of minimum energy $D_{0,ij}$, and α_{ij} is the steepness parameter of the interaction potential. The bond lengths between two bonded beads are constrained by the SHAKE algorithm.[28,29] The resultant forces and coordinate adjustments are naturally applied to the corresponding C1, C4, and C6 atoms. The values of the parameters of all the potential models discussed here are the same as those presented in our previous studies.[14–16]

While the coarse grain M3B model is retained for simulating the conformations of the dextran chains and their intrachain and interchain van der Waals (vdW) interactions, other aspects of dextran interactions with desmopressin, water, ligands, and counterions are desired to be simulated with appropriate atomistic features in order to capture the finer-scale details of the mechanisms responsible for the transport of the charged adsorbate molecule through the electrolytic solution and its adsorption onto the charged ligands in the polymeric porous medium. To fulfill this need, we have followed an approach[27] that generates the coordinates of all the atoms in each dextran chain at every time step based on the ideally optimized structure of a glucose monomer and the instantaneous coordinates of its B1, B4, and B6 beads. The partial charges of the dextran atoms are determined according to the study of Lins and Hünenberger.[30] A hybrid simulation approach is thus utilized in this work where the above coarse grain models and the atomistic models for dextran and for other species discussed below are combined and converged together through the modeling of dextran chains. The united atom approach is further employed to fuse $-CH_3-$, $-CH_2-$, and –CH– groups into pseudoatoms (united atoms)[31–33] and sum the partial charges into group net charges. The Coulombic and vdW interaction centers of the united atoms are placed at the positions of carbon atoms.

The atomistic simulation models for both desmopressin and mercaptopropionic acid are based on the force field developed by Cornell *et al.*[34] who expanded this effort to form AMBER, a simulation package for protein, nucleic acids, and organic molecules. As shown in Fig. 1(a), the H, N, O, S, and C atoms in desmopressin as well as in mercaptopropionic acid are modeled as individual atomistic interaction sites with partial charges.[34–36] The overall net charge of desmopressin (charged adsorbate) is +1e and that of mercaptopropionic acid (charged ligand) is −1e. The $-CH_3-$, $-CH_2-$, and –CH– groups are again modeled as united atoms[31–33] with group net charges and vdW interaction centers placed at the carbon atoms. Each bond in the model desmopressin and ligand molecules is constrained to the equilibrium length by applying the SHAKE algorithm,[28,29] and intramolecular interactions[34–36] have also been simulated, including bond angle bending by $U_{\text{b}}(\theta)=K_\theta(\theta-\theta_{eq})^2$, dihedral torsion by $U_{\text{tor}}(\phi)=\Sigma(V_n/2)[1+\cos(n\phi-\gamma)]$, and nonbonded vdW and Coulombic interactions by

$$\sum_j \sum_{k>j+3}\left\{4\varepsilon_{jk}\left[\left(\frac{\sigma_{jk}}{r_{jk}}\right)^{12}-\left(\frac{\sigma_{jk}}{r_{jk}}\right)^{6}\right]+\frac{1}{4\pi\varepsilon_0}q_jq_k\left[\frac{1}{r_{jk}}+\frac{(1+B_1)}{2}\frac{r_{jk}^2}{r_c^3}\right]\right\}, \tag{3}$$

where the second part of Eq. (3) includes a treatment of the long-range electrostatic interactions ($r_c=12$ Å) based on a generalized reaction field method.[15,16,37]

In our simulation system, the water molecules not only completely cover the dextran chains but also form a bulklike aqueous phase above the dextran layer where the transport of desmopressin starts in the simulation system. For this purpose, a total number of 150 000 water molecules are simulated with a TIP4P model[38] which has been shown to be adequate for simulating thermodynamic properties of dense water systems.[38,39] This model considers each water molecule to be composed of two hydrogen atoms each carrying +0.5564e, one neutral oxygen atom as a vdW interaction center, and one massless site carrying −1.128e in close proximity to the oxygen atom. The interaction forces on the massless sites are decomposed vectorially to the oxygen and hydrogen atoms. The water molecules are simulated as rigid molecules by using the SHAKE[28,29] algorithm to constrain the O–H bonds and the distance between the two hydrogen atoms. The counterions surrounding the ligands or solvated in the aqueous phase are considered to be Na^+ and represented by spherical particles[40] with a point charge and a vdW interaction site at the center. The number of counterions is such that the total amount of charges from ligands and desmopressin is compensated to give the simulation system global electroneutrality. The intermolecular electrostatic and vdW interactions among water, counterion, desmopressin, and ligand molecules are treated in the same manner as indicated by Eq. (3). It is important to note here that although the electrostatic interactions are much more dominant, all the intramolecular and intermolecular vdW interactions discussed above are needed in order to prevent artificial overlap due to Coulombic attractions between opposite charges. These vdW interactions have their parameters determined either directly from the literature[31–36] and/or by using the Lorentz–Berthelot mixing rule when necessary.

The MD simulations in this work are carried out using the leapfrog[29] integration algorithm and a time step $\Delta t=1.0$ fs together with a Gaussian thermostat method[41] to control the temperature at 291 K. A progressive equilibration strategy involving multiple conversion steps and a large number of Δt has been used in order to gradually impart atomistic features into the originally coarse grain model sys-

tem from our previous work[16] without encountering physically implausible interactions. Water molecules are the first to be converted from spherical particles to the atomistic TIP4P model with random initial orientations, while dextran chains, ligands, and counterions are kept frozen during this conversion step. When strong repulsions occur due to random initial orientations, a Monte Carlo based technique is used to adjust the orientations of water molecules in order to expedite the evolution of the simulation system towards more reasonable states. Subsequently, dextran monomers and ligands are switched to the atomistic models but remain frozen first so as to allow the system to adjust to the new condition. Afterwards, the full set of hybrid models discussed above and all degrees of freedom simulated by the hybrid models are activated. In the mean time, a desmopressin molecule equilibrated separately in a bulk phase of water with a structure shown in Fig. 1(a) is incorporated into the simulation system with its center of mass fixed at a location in the bulklike aqueous phase above the porous dextran layer. Since larger pores have higher probabilities for biomolecular transport and adsorption to take place, the selected initial position of the desmopressin molecule in this study is above the biggest pore presented by the dextran porous structure and is at 100 Å from the surface of the base matrix which corresponds to the z position of the outermost ligand plus 1.5 times the cutoff distance of the charge-charge interaction. Sufficient time is given and various structures and potential energies are monitored in order to ensure equilibration before the start of the production run.

The goal of this work is aimed at probing the physics of the whole transport and adsorption process of a representative adsorbate biomolecule toward the immobilized ligands in a polymeric adsorbent medium. The combination of a dense liquid phase, porous adsorbent structure, and the ligands surrounded by counterions carrying the same charge as the adsorbate biomolecule makes this process a very slow one that it requires a complex MD simulation procedure,[42] which employs a large number of particles and atomistic simulation models. It is important to note here that the highly flexible dextran chains and mobile counterions and water molecules make it possible for the polymeric adsorbent medium to possess and evolve through many configurations in time and to respond almost instantaneously and continuously to the progress of desmopressin at any location during its transport and adsorption. Such changes affect in turn the position, shape, and mobility of the desmopressin molecule through mutual interactions, making the system under study to have no static equilibrium states but rather ever-changing dynamic states at any point during the transport and adsorption process of desmopressin inside the polymeric adsorbent medium. In this work, the desmopressin molecule starts its transport process from a location in the bulklike region above the biggest pore of the dextran porous layer. The properties of desmopressin are first characterized at this point that is labeled as location *A*. As the desmopressin molecule descends into the porous adsorbent medium and towards the eventual adsorption site, its properties are characterized at five selected points labeled as locations *B*, *C*, *D*, *E*, and *F* along the transport pathway. The z positions and the distances to the closest ligand of the desmopressin molecule for these locations are summarized in Table I. Eventually the desmopressin molecule arrives at z=50.6 Å and falls into a state that can be reasonably considered to be the start of desmopressin adsorption. This state is labeled as location *G* and, as will be discussed below, is not a singular state but one that encompasses further structural and energetic evolution.

TABLE I. Distances to the surface (z) and to the closest ligand (d) from the desmopressin center of mass and the hydrodynamic radius and the radius of gyration of desmopressin at different locations along its transport pathway and at its adsorption site.

Location	z (Å)	d (Å)	Hydrodynamic radius (Å)	Radius of gyration (Å)
A	93.9	54.1	9.5	2.3
B	78.5	39.6	13.9	3.1
C	65.8	20.1	10.2	3.1
D	67.0	15.6	9.1	3.4
E	56.2	11.9	12.2	3.6
F	49.4	8.0	12.0	3.6
G	50.6	5.0	11.1	3.6
H	36.4	2.7	14.7	5.3

III. RESULTS AND DISCUSSION

It should be emphasized first that in addition to thermal diffusion, electrophoretic[9] migration due to the presence of an electric field resulting from nonuniform distributions of charged species also affects the displacement of a biomolecule and thus contributes to its transport rate. As a result, when both contributions are present simultaneously as in the adsorption system under study in this work, the effective rate of biomolecular transport is more reasonable to be described as being characterized by a mass transport coefficient instead of a thermal diffusion coefficient. Since both thermal diffusion and electrophoretic[9] migration contribute to the displacement of desmopressin, the magnitude of the effective mass transport coefficient, $(\mathrm{MT})_z$, is reflected in the mean square displacement and could thus be characterized, as a first order approximation, by the following expression:[28,35,36]

$$\langle (z_{\mathrm{com}}(t+t_0) - z_{\mathrm{com}}(t_0))^2 \rangle = 2(\mathrm{MT})_z t, \tag{4}$$

where z is designated to be the direction of net transport, z_{com} is the instantaneous z position of desmopressin center of mass, and $(\mathrm{MT})_z$ denotes the effective mass transport coefficient. In a system with a flat and homogeneous surface and no flexible porous layer, the differences in the values of the biomolecule effective mass transport coefficient have been found and shown in Refs. 35 and 36 to be mainly a function of the distance from the charged interface. However, because polymeric dextran chains are flexible and anchored on a nonflat surface and the spatial density distribution of the immobilized ligands is nonuniform,[16] the resultant porous adsorbent medium in the present work, as shown in Fig. 1, has such significant inhomogeneity that the transport of the adsorbate biomolecule (desmopressin) in the porous medium exhibits complex dynamic behavior with dependencies on all directions. To accomplish a reasonable analysis in a timely

TABLE II. Effective mass transport coefficient, $(MT)_z$, of desmopressin at different locations along its transport pathway.

Location	$(MT)_z$ (m^2/s)
A	4.57×10^{-10}
B	1.15×10^{-10}
C	1.55×10^{-10}
D	1.98×10^{-10}
E	2.03×10^{-10}
F	7.15×10^{-11}

manner, the transport of the desmopressin molecule in this work is characterized by the effective mass transport coefficients evaluated according to Eq. (4) for the six selected locations along the pathway that desmopressin traveled. The results are tabulated in Table II and show that in location *A* where desmopressin is immersed in a bulklike phase, its effective mass transport coefficient is found to be 4.57×10^{-10} m^2/s, which interestingly is in good agreement with that of desmopressin in a similar bulk phase in a recent study,[35] despite the differences between the simulation systems and potential models; in fact, the value is very close to the experimentally[35] determined value of 3.94×10^{-10} m^2/s. Judging by the general trend of the results in Table II, it is apparent that one of the effects of the porous medium is to cause the desmopressin molecule to have decreased effective mass transport coefficients during its transport inside the porous layer. Zhang *et al.*[35] have shown that when desmopressin descends towards the substrate surface, a flat surface with a significant surface density of charged ligands and without counterions or a porous layer has a strong effect of electrophoretic[9] migration to cause the effective mass transport coefficient of desmopressin to increase significantly. However, in the porous adsorbent medium considered in this work, the charged ligands are immobilized on the dextran chain molecules having a high level of conformational flexibility and are surrounded by counterions. As a consequence, the effect of electrophoretic[9] migration on desmopressin is less significant, although a slight increase in the effective mass transport coefficient is observed as the desmopressin molecule approaches a ligand from location *B* to location *E*. In location *F*, the value of the effective mass transport coefficient decreases again because the desmopressin molecule is ready to be adsorbed and, thus, it is under the influence of strong interactions with the adsorption site that limit its mobility.

One of the main factors affecting the effective mass transport coefficient of the desmopressin molecule is its instantaneous local environment. In order to further analyze this aspect, we compute the radial distributions of ligands, counterions, and charges with respect to the center of mass of the desmopressin molecule and plot them in Figs. 2 and 3. For better comparison and elucidation, we also examine the shapes and conformations of the desmopressin molecule of which six are shown in Fig. 4 for locations *A*, *C*, and *G*. The distributions of charges in Figs. 2 and 3 include all positive, negative, and partial charges from ligands, counterions, and water molecules. At larger radial distances from desmopressin, these various charges gradually neutralize each other and result in diminished charge density, while within immediate distances from desmopressin most of the contributions to the charge density come from water molecules surrounding desmopressin whose orientations and structures can actually be revealed by the characteristics of the first few peaks. In locations *A* through *C* as shown in Fig. 2, there is no ligand or counterion within 20 Å from desmopressin because the molecule of desmopressin is either in the bulklike phase above the dextran layer or in a big pore located in the outer region of the dextran layer whose radius is greater than 100 Å. However, significant differences can be seen in the distributions of charges due to water molecules between location *A* and location *C* because in location *A* in the bulklike region desmopressin maintains a more compact structure (cf. Fig. 4) and the distribution of the surrounding water molecules are not substantially disturbed, while in location *C* desmopressin has changed to a more elongated shape (cf. Fig. 4) inside the pore which together with the confinement effect of the pore space causes the water molecules to behave differently around desmopressin. The larger magnitudes and the sign of the first major peak of the charge distribution in location *C* suggest that the water molecules tend to be better packed and have more specific orientations with their positively charged hydrogen atoms pointing toward desmopressin. Judging by the characterization in the locations presented in Figs. 2 and 3, the water molecules appear to be more ordered and form a tighter network in the proximity of

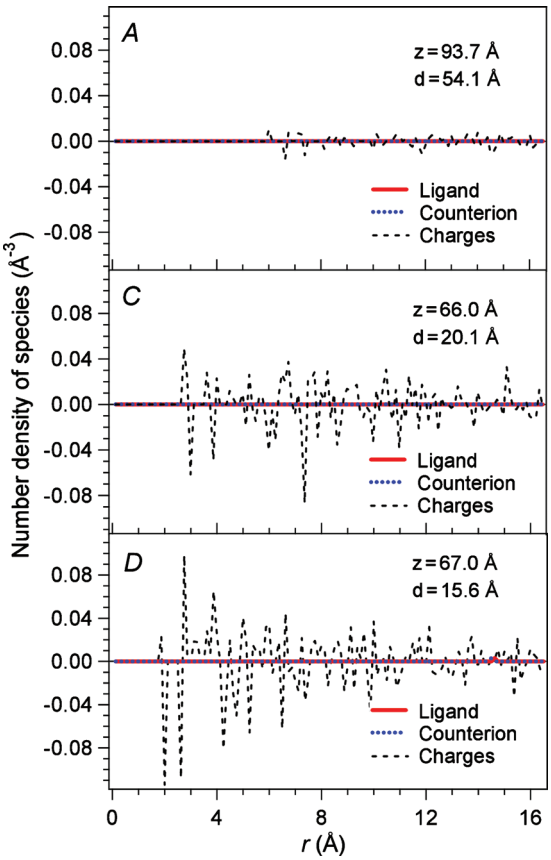

FIG. 2. Radial distributions from the desmopressin center of mass of the number densities of ligands, counterions, and sum of charges in locations *A*, *C*, and *D* defined in the text and in Table I.

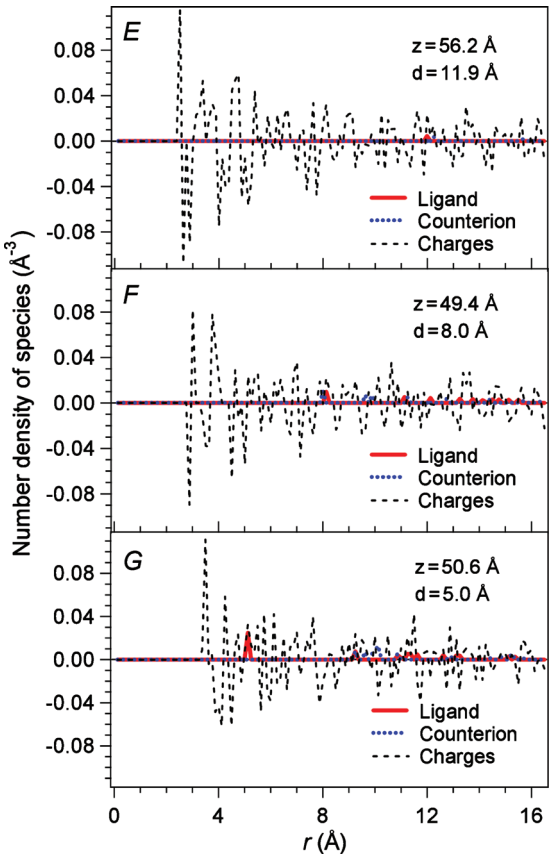

FIG. 3. Radial distributions from the desmopressin center of mass of the number densities of ligands, counterions, and sum of charges in locations *E*, *F*, and *G* defined in the text and in Table I.

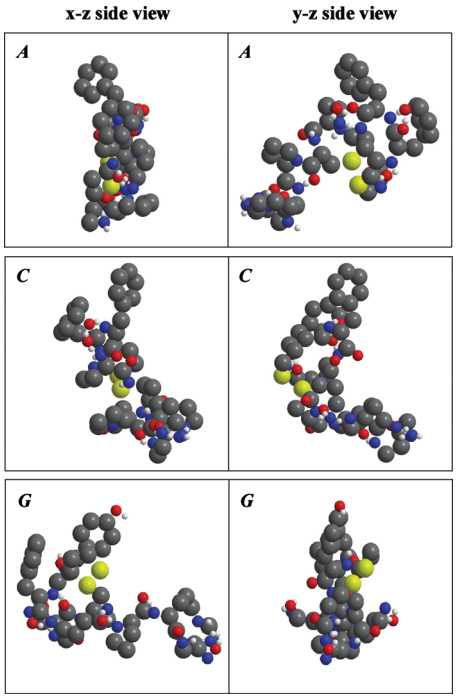

FIG. 4. Side views of the desmopressin molecule in locations *A*, *C*, and *G*. The red, blue, yellow, and light gray beads represent O, N, S, and H atoms, respectively, and the dark grey beads represent C atoms or CH, CH_2, and CH_3 pseudoatoms.

the desmopressin molecule in the porous medium, which could be considered as one of the causes underlying the decreased effective mass transport coefficients of desmopressin.

Beyond location *C*, the closest ligands to the desmopressin molecule show up in the figures at radial distances denoted by d in the figures. As indicated by the results in Figs. 2 and 3, the distributions of ligands and counterions are mostly tied closely together, reflecting the fact that the ligands are surrounded by counterions with opposite charges. However, from location *F* to location *G* in Fig. 3, the counterion originally attached to the closest ligand is displaced as desmorepssin approaches from a preadsorption state to become adsorbed. Since the immediate charge distributions surrounding desmopressin are dominated by water molecules, the starting point of a charge distribution can be taken as the smallest radius of desmopressin from its center of mass, which in turn can be used as an indication of whether the desmopressin molecule has changed conformation and shape. From this point of view, Figs. 2 and 3 indicate that the smallest radius of the desmopressin molecule is ~6 Å in the bulk phase and decreases to 2–3 Å in the porous medium, which means that the adsorbate molecule changes its shape to become more elongated during its transport toward an adsorbent ligand. These structures and structural changes are consistent with the side views of simulation snapshots shown in Fig. 4, which also demonstrate the orientational changes of the desmopressin molecule. Moreover, the hydrodynamic radius and the radius of gyration of desmopressin have also been calculated and included in Table I at different positions with respect to the agarose surface and the closest ligand. It is apparent that these radii also change significantly as desmopressin is induced by the surroundings in the porous medium to change shape. Therefore, in macroscopic modeling studies where the mathematical models employ similar porous media and hydrodynamic radius and/or radius of gyration as parameters, it would be more desirable and more accurate to include the possibilities of radius variations at least as a function of the distance from the substrate surface.

Due to its size and its van der Waals and Coulombic interactions directly with dextran monomers and indirectly with counterions and water, the presence of the desmopressin molecule can certainly be expected to further modify the porous structure of the dextran layer. To dissect this phenomenon, we consider the distributions of B4 beads, ligands, counterions, pore openings, and pore volume in the *z* direction from the surface of the agarose base matrix. As shown by Figs. 5(a), 6(a), 7(a), and 8(a), the bulk of the dextran monomers concentrates to the region between 20 and 45 Å from the surface of the agarose base matrix. A high density of dextran monomers in this region naturally results in only smaller pores and also presents a steric effect to prevent the activated B4 beads from being completely accessible to the immobilization of the ligands. This has been demonstrated in detail in our previous study[14] and provides the reason about the less than 100% loading of the ligands in the region between 20–45 Å from the agarose surface. On the other hand, the upper region of the dextran porous layer has a ligand loading close to 100%. At the outermost region of the dextran layer, there exist the largest pore opening and pore vol-

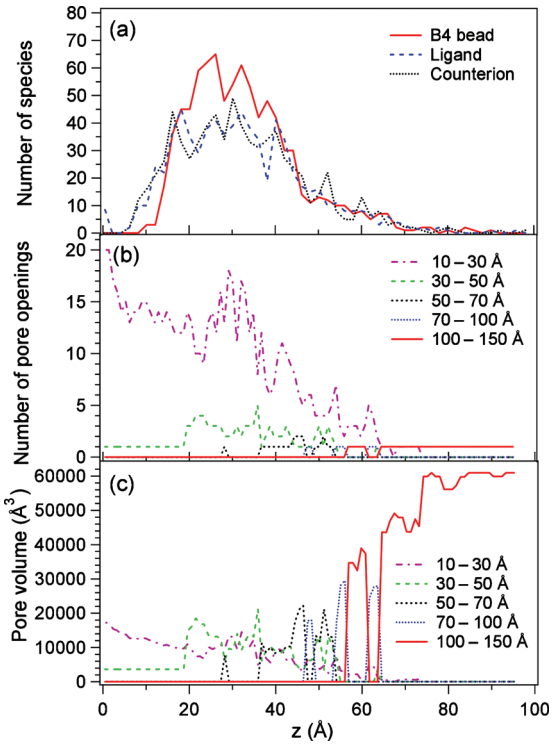

FIG. 5. Distributions of the (a) number of B4 beads, ligands, and counterions, (b) number of pore openings, and (c) pore volume along z (which represents the direction of net transport) in location A. Pores of different radii are categorized based on the size ranges shown on the figures.

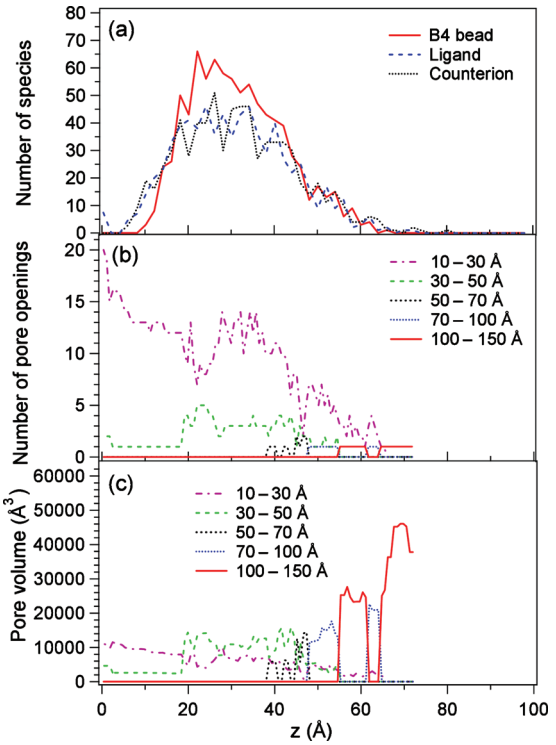

FIG. 7. Distributions of the (a) number of B4 beads, ligands, and counterions, (b) number of pore openings, and (c) pore volume along z (which represents the direction of net transport) in location F. Pores of different radii are categorized based on the size ranges shown on the figures.

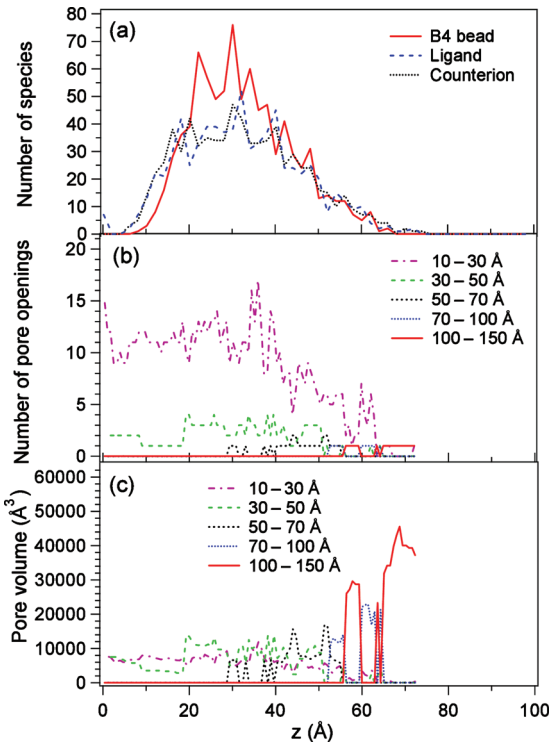

FIG. 6. Distributions of the (a) number of B4 beads, ligands, and counterions, (b) number of pore openings, and (c) pore volume along z (which represents the direction of net transport) in location C. Pores of different radii are categorized based on the size ranges shown on the figures.

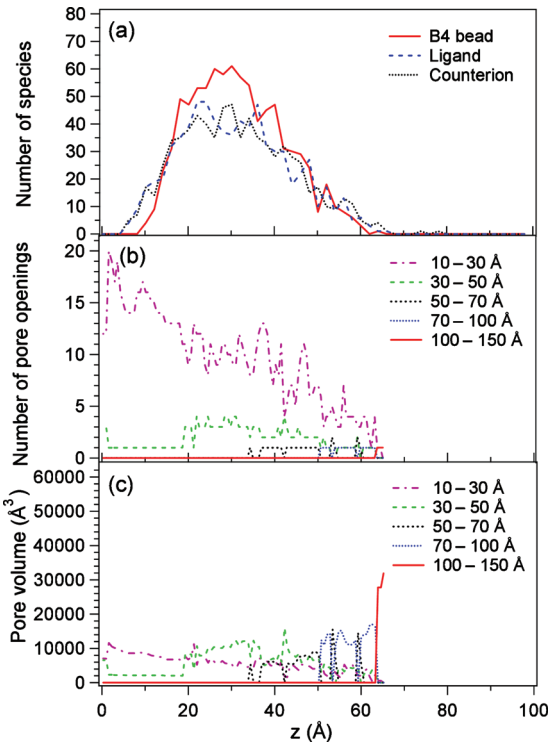

FIG. 8. Distributions of the (a) number of B4 beads, ligands, and counterions, (b) number of pore openings, and (c) pore volume along z (which represents the direction of net transport) in location G. Pores of different radii are categorized based on the size ranges shown on the figures.

ume that are caused by a segment of a dextran chain dangling above the rest of the dextran chains. However, because of the flexibility and mobility of the dextran chains, this largest pore can extend significantly above the bulk of the dextran layer or withdraw and become close to the dextran layer at different times. For the same reason, this largest pore can decrease and increase its pore radius as it extends into the dextran porous layer, which has been shown clearly in Figs. 5–8 by the rises and falls alternating between the size range of 100–150 Å and the size range of 70–100 Å in the distributions of pore number and pore volume. In fact, smaller pores also change their pore radii as they extend through the porous layer. In general, the largest pore ends at around 50 Å from the agarose surface, which happens to be the location of the adsorption of desmopressin, but there is still a good level of pore connectivity[14–16] in the porous medium to permit relatively small adsorbates under proper conditions to reach the lower regions. We found that when the adsorption process starts which is location *G* presented in Fig. 8, the z position of desmopressin corresponds to the end of the large pore in the size range of 70–100 Å. The adsorption of desmopressin can be seen to decrease the thickness of the dextran layer and reduce the pore volume in the porous medium that could have significant effects on the subsequent transport and adsorption of additional desmopressin molecules. In particular, the adsorbed desmopressin can block at least partially certain pores connected to the regions adjacent to the adsorption site, thereby hindering the availability of certain ligands there for further adsorption. These effects together can be reasonably categorized as volume exclusion effects.

It is observed in our simulations that it takes repeated attempts for the desmopressin molecule to approach a ligand and finally become adsorbed. In the meantime, the ligand on which desmopressin is to be adsorbed and more importantly the counterions nearby the ligand adjust dynamically in order to accommodate the charged adsorbate molecule of desmopressin which is bigger than an individual ligand or counterion. To capture such dynamic adjustments in a quantitative manner, we consider and calculate the distributions of ligands, counterions, and water molecules within a cylindrical space of 13 Å in diameter between desmopressin and the ligand on which desmopressin is adsorbed. Compared to the radial distributions in Figs. 2 and 3 that survey the local environment in all directions around the desmopressin molecule, the cylindrical distributions provide a probe window focused on the mutual influences between the incoming desmopressin molecule and the adsorption site that contains the ligand and accompanying counterions. The resultant cylindrical distributions are shown in Figs. 9 and 10 as a function of the distance, z_{cyl}, along the axial direction of the cylindrical space between the desmopressin center of mass and the C atom in the COO^- group of the ligand. Because the ligand and the dextran monomers have certain sizes and conformational flexibility, the starting point of z_{cyl} is placed 8.7 Å behind the C atom in the COO^- group of the ligand in order to provide more complete views. In addition, the bulk density of water has been converted from 1.0 g/cm^3 to 0.0334 water molecules per $Å^3$ and plotted with thick dotted lines as a reference in Figs. 9 and 10. In general, there are decreased

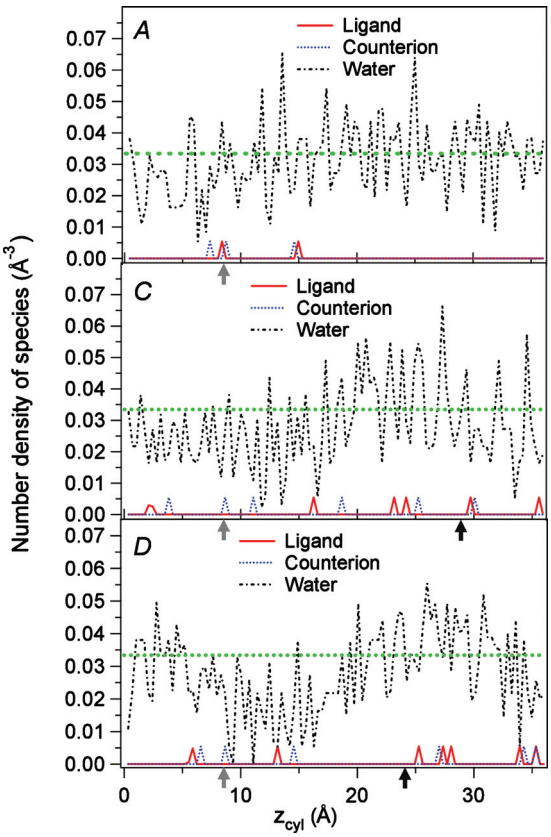

FIG. 9. Cylindrical distributions of the number densities of ligands, counterions, and water molecules in locations *A*, *C*, and *D* where the position of the C atom in the closest COO^- group and that of the desmopressin center of mass are indicated by the gray and black arrows, respectively.

levels of water density at axial distances smaller than ~10 Å, which is evidently due to the excluded volumes of the ligand and the nearby counterions. In location *A* in Fig. 9 where the desmopressin molecule is more than 94 Å away from the ligand and in a bulklike phase, the water molecules probed by the cylindrical distribution are mostly those contained in the porous medium and they are shown to be able to form a liquid structure with much the same density as the bulk density of water in the absence of adsorbate molecules. In location *C* where desmopressin has entered the porous layer and is located at a relatively short distance d=20.1 Å to the closest ligand, more counterions are detected within the cylindrical space and some of them are clearly not associated with ligands. These "free" counterions can be understood to be displaced from ligands due to the presence of desmopressin that carries the same type of charge as the counterions and thus exerts repulsion on the nearby counterions. They can also be seen to be present in locations *D* and *E* in Figs. 9 and 10. It should be emphasized here that being covalently bonded to the dextran chains, the ligands cannot become free as the counterions. Nevertheless, the free counterions, the desmopressin molecule, and the flexibility of the dextran chains can interact together to change the cylindrical distribution of ligands constantly. Desmopressin in location *F* has an elongated structure (cf. Table I) toward the ligand that will be involved in its adsorption, which significantly decreases the number of water molecules along the adsorption pathway. Eventually desmopressin establishes direct in-

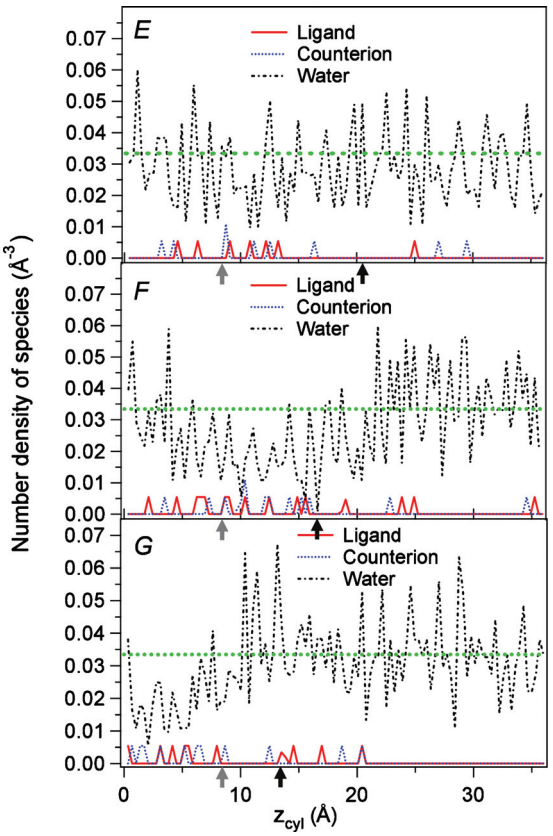

FIG. 10. Cylindrical distributions of the number densities of ligands, counterions, and water molecules in locations *E*, *F*, and *G* where the position of the C atom in the closest COO^- group and that of the desmopressin center of mass are indicated by the gray and black arrows, respectively.

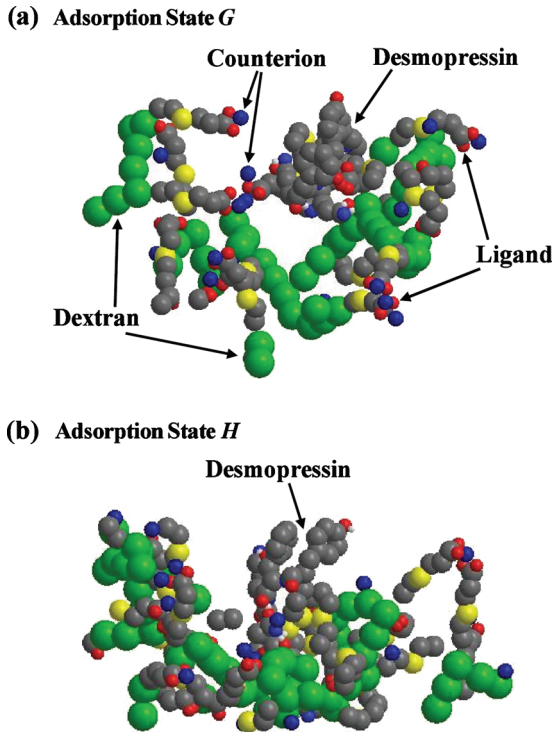

FIG. 11. Side views of the desmopressin-ligand complex in the adsorbed states characterized as locations *G* and *H*.

teraction with the ligand in location *G* and the water molecules outside the region of distances that are very close to the desmopressin-ligand complex are able to relax back to their bulklike density.

An important finding in this work is that in the porous adsorbent medium considered here, adsorption is found to be a process instead of a single state due mainly to the flexibility of the dextran chains. Starting from location *G*, we found that the adsorption complex continues to evolve slowly and after 800 ps it has reached a state that has a very different structure and very different interaction energetics. For better clarification and easier comparison, this later state of adsorption is labeled as location *H* in the following discussion. The structural change from location *G* to location *H* can be clearly demonstrated by the simulation snapshots shown in Fig. 11 and by the radial distributions presented in Fig. 12 of the species involved in the formation of the desmopressin-ligand complex. From Fig. 11, it is evident that the structure of the desmopressin-ligand complex in location *H* is significantly more compact and possesses more contacts with the dextran chains and the ligands than that at the beginning of the adsorption process in location *G*. The interactions of desmopressin with the flexible dextran chains and the structural evolution of the desmopressin-ligand complex can certainly alter further the porous structure of the adsorbent medium at least locally. An examination of Fig. 12 can provide a quantitative assessment in this aspect. It is found that within the same spherical space from the center of mass of the adsorbed desmopressin, not only significantly more dextran monomers, ligands, and counterions are present, but also they are much closer to the adsorbed desmopressin at a later adsorption stage (location *H*) than at the beginning of adsorption (location *G*). This also implies a more compact desmopressin-ligand complex in location *H* and confirms the finding based on visualization. When the dextran chains are induced to change their structures to have more monomers close to a single adsorbate molecule, the structural changes can shield certain ligands from being available to subsequent adsorbate molecules, resulting in a type of volume exclusion

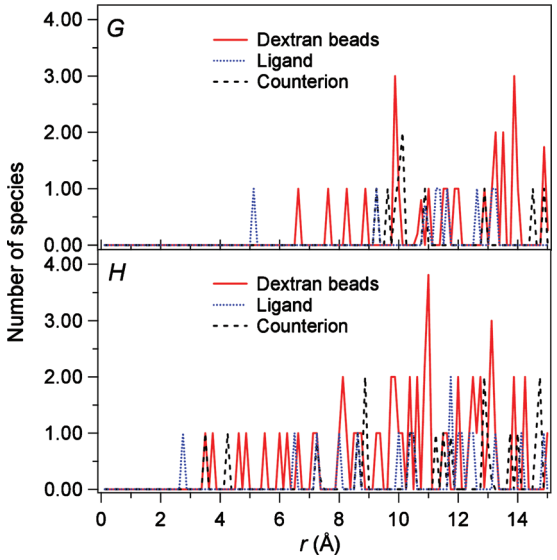

FIG. 12. Radial distributions from the desmopressin center of mass of the numbers of dextran monomers, ligands, and counterions in the adsorbed states characterized as locations *G* and *H*.

effect. The fact that the adsorption of a biomolecule is a process in the adsorbent medium and that the adsorbate and the porous structure of the adsorbent medium mutually affect each other can be easily envisioned[14–16] to have significant implications to the design and construction of adsorbent particles for effective bioseparations and to the synthesis and operation of such bioseparation processes.

In location *F* that is considered to represent a state on the verge of adsorption, the distance is 8 Å between desmopressin and the closest ligand (cf. Table I). It is important to point out that within the same distance of 8 Å from its center of mass, the desmopressin molecule in location *G* has only one ligand as shown in Fig. 12, meaning that the adsorption is of one-site interaction in nature when it starts. However, the desmopressin molecule in location *H* has three ligands within 8 Å from its center of mass, meaning that the nature of the adsorption has changed and involved multisite interactions after 800 ps from location *G*. It is thus considered to be possible that when there is continuous adsorption of desmopressin molecules in the adsorbent medium, one-site interaction and multisite interactions would coexist and the transition from the former to the latter can take place continuously. Such a transition from one-site interaction to multisite interactions reduces the overall adsorption capacity of the ligands and the adsorbent medium, which phenomenologically can be considered as a type of surface exclusion effect. It may also cause inner radial humps[43] in the concentration profile of the molecules adsorbed by multisite interactions. These phenomena as well as other important practical implications have been discussed in Refs. 24, 43, and 44. Based on the results and discussion presented here and in our previous studies,[14–16] it can be stated that using stiff extender chain molecules and low levels of ligand loading could minimize the occurrence of multisite interactions in similar adsorption systems. It could also be possible that in a porous adsorbent medium constructed with flexible polymeric extender chains, the effects of the surface and volume exclusion phenomena due to the adsorption of the first batch of adsorbate biomolecules could adversely change the pore structure to such an extent that the porous adsorbent medium may no longer be desirable for subsequent adsorption of additional adsorbate molecules and for the overall separation process. However, such surface and volume exclusion effects could also be capable of transforming a previously less desirable porous adsorbent structure into a certain new structure that exhibits better overall bioseparation performance. Therefore, for rational design of optimal porous adsorbent media for bioseparations, it is important and even necessary in practice and in employing the methodology developed through our previous studies[14–16] and the present work to adopt an iterative strategy that returns to stages I and II[14–16] to generate other porous structures for the adsorbent media which could be constructed with different sets of system parameters and may even consider different types of counterions and immobilized ligands, and then an examination of their performance with respect to the transport and adsorption of the adsorbate biomolecules of interest in stage III would have to be undertaken. With sufficient personnel support and computing facilities, this iterative strategy can be greatly facilitated by generating a range of porous structures in stage I,[14] immobilizing the ligands in stage II,[15,16] and assessing their adsorption separation performance in stage III simultaneously.

IV. CONCLUSIONS AND REMARKS

Bioseparations based on ion-exchange chromatography can be considered to be consisted of three stages, where stage I concerns itself with the construction of the porous adsorbent medium formed from the mutual interaction of the polymeric extender molecules grafted on the pore surface of the base matrix and stage II involves the immobilization of ligands onto the porous polymeric adsorbent medium obtained in stage I. In this work, the transport of a charged adsorbate biomolecule (desmopressin) in the porous polymeric adsorbent medium and its adsorption onto the immobilized ligands (mercaptopropionic acid), namely, stage III, have been modeled and studied using molecular dynamics modeling and simulations.

In the porous adsorbent medium, the biomolecule is found to change shape, orientation, and lateral position in order to proceed toward the adsorption site. Furthermore, its effective mass transport coefficient is lower than the value in the bulk phase as the adsorbate approaches closer to the immobilized ligand. In porous adsorption systems, apart from the effect imposed on the effective mass transport coefficient of the adsorbate molecule by the networked structure of the water molecules surrounding the adsorbate molecule, additional factors that have important influences on the magnitude of the effective mass transport coefficient of the adsorbate molecule could include (a) the shape of the adsorbate molecule, (b) the repulsion on the adsorbate molecule from the counterions that have the same type of charge as the adsorbate molecule, and (c) the possible intervening interactions of the charged species, including thereby the adsorbate molecule, with the polymer chains forming the surfaces of the pores of the adsorbent medium that could lead to confinement of space resulting in a smaller degree of freedom of movement of the adsorbate molecule in the pore due also to the shape of the adsorbate molecule. Furthermore, because the counterions surrounding the ligands carry the same type of charge as the adsorbate biomolecule, it takes the adsorbate biomolecule repeated attempts to approach toward a ligand in order to displace the counterions and finally become adsorbed. The adsorbate-ligand complex interacts with other vacant ligands, the counterions, and the polymeric extender molecules and it is found to start as one-site interaction but slowly and continuously evolves toward multisite interactions. Such a transition from one-site interaction to multisite interactions reduces the overall adsorption capacity of the immobilized ligands and the adsorbent medium, which can be considered as a type of surface exclusion effect. In addition, the adsorption of the biomolecule also presents volume exclusion effects by being able to not only directly reduce the pore volume and the availability of the ligands in the adjacent pores, but to also induce the polymeric extender molecules through mutual interactions to change to more compact structures that could shield certain ligands from be-

ing accessible to subsequent adsorbate molecules. The insights and findings from this work could have significant implications on the fundamental side to the relevant macroscopic modeling studies regarding their constitutive equations and parameter values, and on the practical side to the design and construction of the polymeric porous adsorbent media for effective bioseparations and to the synthesis and operation of bioseparation processes employing such porous adsorbent media.

It is worth mentioning here that the methodology developed by our recent work[14–16] and this study together encompasses a set of modeling, simulation, and analysis methods for investigating various stages in the separation of biomolecules. They could also be suitable, individually or together, for the study of biocatalysis, especially the behavior of the transport of the substrate molecule in the porous catalytic medium, its adsorption onto the immobilized enzyme, and the behavior of the desorption and the transport of the product molecule produced by the conversion of the substrate, which represent the rather slow steps of enzymatic catalysis.

[1] R. G. Harrison, P. Todd, S. R. Rudge, and D. R. Petrides, *Bioseperation Science and Engineering* (Oxford University Press, New York, 2003).
[2] C. F. Poole, *The Essence of Chromatography* (Elsevier, Amsterdam, 2003).
[3] H. Berg, H. Hansson, and L. Kagedal, "Adsorption/separation method and a medium for adsorption/separation," U.S. Patent No. 6,428,707 B1, 6 August 2002.
[4] A. I. Liapis, B. A. Grimes, K. M. Lacki, and I. Neretnieks, J. Chromatogr. A **921**, 135 (2001).
[5] X. Zhang, B. A. Grimes, J.-C. Wang, K. M. Lacki, and A. I. Liapis, J. Colloid Interface Sci. **273**, 22 (2004).
[6] B.-L. Johansson, M. Belew, S. Eriksson, G. Glad, O. Lind, J.-L. Maloisel, and N. Norman, J. Chromatogr. A **1016**, 21 (2003).
[7] B.-L. Johansson, M. Belew, S. Eriksson, G. Glad, O. Lind, J.-L. Maloisel, and N. Norman, J. Chromatogr. A **1016**, 35 (2003).
[8] X. Zhang, J.-C. Wang, K. M. Lacki, and A. I. Liapis, J. Phys. Chem. B **109**, 21028 (2005).
[9] A. I. Liapis and B. A. Grimes, J. Sep. Sci. **28**, 1909 (2005).
[10] C. Harinarayan, J. Mueller, A. Ljunglöf, R. Fahrner, J. M. Van Alstine, and R. van Reis, Biotechnol. Bioeng. **95**, 775 (2006).
[11] A. I. Liapis and B. A. Grimes, J. Sep. Sci. **30**, 648 (2007).
[12] A. Ljunglöf, K. M. Lacki, J. Mueller, C. Harinarayan, R. van Reis, R. Fahrner, and J. M. Van Alstine, Biotechnol. Bioeng. **96**, 515 (2007).
[13] A. I. Liapis and B. A. Grimes, Sep. Purif. Technol. **59**, 342 (2008).
[14] E. Riccardi, J.-C. Wang, and A. I. Liapis, J. Phys. Chem. B **112**, 7478 (2008).
[15] E. Riccardi, J.-C. Wang, and A. I. Liapis, J. Phys. Chem. B **113**, 2327 (2009).
[16] E. Riccardi, J.-C. Wang, and A. I. Liapis, J. Chromatogr. Sci. **47**, 459 (2009).
[17] M. Sahimi, G. R. Gavalas, and T. T. Tsotsis, Chem. Eng. Sci. **45**, 1443 (1990).
[18] A. I. Liapis, Math. Model. Sci. Comput. **1**, 3 (1993).
[19] F. A. L. Dullien, *Porous Media: Fluid Transport and Pore Structure* (Academic, New York, 1992).
[20] D. Stauffer and A. Aharony, *Introduction to Percolation Theory* (Taylor and Francis, London, 1992).
[21] J. J. Meyers and A. I. Liapis, J. Chromatogr. A **827**, 197 (1998).
[22] J. J. Meyers and A. I. Liapis, J. Chromatogr. A **852**, 3 (1999).
[23] J. J. Meyers, O. K. Crosser, and A. I. Liapis, J. Biochem. Biophys. Methods **49**, 123 (2001).
[24] E. Riccardi, J.-C. Wang, and A. I. Liapis, J. Sep. Sci. **32**, 3084 (2009).
[25] A. Ljunglöf and J. Thömmes, J. Chromatogr. A **813**, 387 (1998).
[26] B. Walse, J. Kihlberg, and T. Drakenberg, Eur. J. Biochem. **252**, 428 (1998).
[27] V. Molinero and W. A. Goddard, J. Phys. Chem. B **108**, 1414 (2004).
[28] D. C. Rapaport, *The Art of Molecular Dynamic Simulation* (Cambridge University Press, New York, 1995).
[29] M. P. Allen and D. J. Tildesley, *Computer Simulation of Liquids* (Clarendon, Oxford, 1987).
[30] R. D. Lins and H. H. Hünenberger, J. Comput. Chem. **26**, 1400 (2005).
[31] S. J. Weiner, P. A. Kollman, D. A. Case, U. C. Singh, C. Ghio, G. Alagona, S. Profeta, and P. Weiner, J. Am. Chem. Soc. **106**, 765 (1984).
[32] L. Dunfield, A. Burgess, and H. Scheraga, J. Phys. Chem. **82**, 2609 (1978).
[33] W. Jorgensen, J. Am. Chem. Soc. **103**, 335 (1981).
[34] W. D. Cornell, P. Cieplak, C. I. Bayly, I. R. Gould, K. M. Merz, Jr., D. M. Ferguson, D. C. Spellmeyer, T. Fox, J. W. Caldwll, and P. A. Kollman, J. Am. Chem. Soc. **117**, 5179 (1995).
[35] X. Zhang, J.-C. Wang, K. M. Lacki, and A. I. Liapis, J. Colloid Interface Sci. **277**, 483 (2004).
[36] X. Zhang, J.-C. Wang, K. M. Lacki, and A. I. Liapis, J. Colloid Interface Sci. **290**, 373 (2005).
[37] I. G. Tironi, R. Sperb, P. E. Smith, and W. F. van Gunsteren, J. Chem. Phys. **102**, 5451 (1995).
[38] J. L. F. Abascal and C. Vega, J. Chem. Phys. **123**, 234505 (2005).
[39] M. Martin-Conde, L. G. MacDowell, and C. Vega, J. Chem. Phys. **125**, 116101 (2006).
[40] A. Grossfield, P. Ren, and J. W. Ponder, J. Am. Chem. Soc. **125**, 15671 (2003).
[41] D. Brown and J. H. R. Clarke, Mol. Phys. **51**, 1243 (1984).
[42] E. Riccardi, Ph.D. dissertation, Department of Chemical and Biological Engineering, Missouri University of Science and Technology, Rolla, Missouri, 2009.
[43] B. H. Arve and A. I. Liapis, AIChE J. **33**, 179 (1987).
[44] B. H. Arve and A. I. Liapis, Biotechnol. Bioeng. **32**, 616 (1988).